Electronic Supplementary Material (ESI) for Chemical Communications.
This journal is © The Royal Society of Chemistry 2018

Electronic Supplementary Information

Re-designing the α-synuclein tetramer

Liang Xu, Shayon Bhattacharya, Damien Thompson*

Department of Physics, Bernal Institute, University of Limerick, V94 T9PX, Ireland.

Corresponding author E-mail: Damien.thompson@ul.ie; Tel: +353 61237734

Contents

Methods…….....Page S2
Fig. S1. MD simulations of different helical NAC tetramers (T1–T4) …….....Page S3
Fig. S2. MD simulations of a helical βS NAC tetramer …….....Page S4
Fig. S3. MD simulations of the tetramer **T3** ……Page S5
Fig. S4. The fraction of native contacts Q for different αS tetramers ….....Page S6
Fig. S5. The time change of helix structures over 200-ns simulations of different αS tetramers……Page S7
Fig. S6. Distribution of conformational energy calculated for different αS tetramers……Page S7
Fig. S7. MD simulations of a βS tetramer……..……..Page S8
Fig. S8. Contact maps for different tetramers……...Page S9
Fig. S9. MD simulations of different helical NAC tetramers after 200-ns simulation of the full-length tetramers…….....Page S10
Fig. S10. Pearson Correlation Coefficient (P.C.C) between conformational energy and different interaction energies……...Page S11
Fig. S11. MD simulations of helical α and β monomers……Page S12
Fig. S12. Number of protein-water hydrogen bond for residues of interest……...Page S13
Fig. S13. The correlation function of protein-water hydrogen bond for residues of interest……Page S14
Fig. S14. Comparison of $^{3}J_{HNH\alpha}$ coupling constant, Hα and N chemical shifts……..Page S15
Table S1. Conformational energy calculated using the GBMV implicit model……Page S16
Table S2–Table S5. P.C.C. of J-coupling constants and chemical shifts between different systems……Page S17
References…….....Page S18

Methods

The initial structures of helical αS tetramers **T1**, **T2**, **T3** and **T4** (**Fig. 2**) were generated as follows. **T1** was constructed by packing the membrane-bound αS structure (PDB ID: 1XQ8);[1] **T2** was taken from previous simulation results of αS multimers;[2] **T3** was provided by Dr. Thomas Pochapsky;[3] and **T4** was designed in terms of available experimental evidence about the loop region connecting α1 and α2 segments in helical αS tetramers.[4] Except **T2**, the other three tetramers are homogeneous tetramers. **M1**, **M3**, and **M4** were monomers used to construct **T1**, **T3**, and **T4**, and directly used in the control monomer simulations; whereas **T2** is a heterogeneous tetramer, and only one of its monomers was used in simulations of **M2**. The starting NAC tetramers were taken from the corresponding tetramers. The initial structures of βS monomer and tetramer were constructed based on **M4** and **T4**. A set of mutations (E46K, H50Q, G51D and A53T) were introduced simultaneously in each monomer, resulting in four mutant monomers **M1_M**, **M2_M**, **M3_M** and **M4_M**, and four mutant tetramers **T1_M**, **T2_M**, **T3_M**, and **T4_M**. Note that the wild type αS monomer has a negative charge of -9e. The quadruple mutant (E46K + H50Q + G51D + A53T) in the loop motif has a net charge of -8e. The change of the protein charge (-4e) in the tetramer could lead to considerable change in the electrostatic interactions and polar contribution to the solvation energy (see Table S1).

All protein structures were represented by the CHARMM36m force field,[5] and the corresponding modified TIP3P water model was used to solvate the protein structure. Molecular dynamics (MD) simulations were performed using GROMACS-5.0.4 software.[6] Each structure was solvated in a water box, with any protein atom at least 15 Å from the box edge, and salt ions were added to neutralize formal charge with an additional 0.15 M NaCl to represent physiological ionic strength. MD simulations were conducted at 310 K and 1 atm. The temperature was maintained using a velocity rescaling thermostat,[7] and the pressure was controlled by the Parrinello-Rahman coupling method.[8] The short-range van der Waals and electrostatic interactions were truncated using a cut-off of 12 Å, and the long-range electrostatics treated using the particle mesh Ewald (PME) method. Each system was first subjected to energy minimization, followed by two stages of equilibration with positional restraints on the heavy atoms of the protein structure: 100 ps at constant volume followed by 100 ps at constant pressure at 310 K. A time step of 2 fs was applied with the LINCS algorithm. Production dynamics were then performed at constant pressure without any positional restraints, with the trajectory saved every 10 ps.

The conformational energy was calculated using the Generalized Born using Molecular Volume (GBMV) implicit solvent model implemented in the CHARMM (v40b2) program.[9] The single point energy was calculated after 200-step minimization of each conformation using the GBMV II algorithm.[10] Other energy terms including bonded energy, van der Waals energy, electrostatic energy, and solvation energy were also obtained with the GB implicit solvent model. The block average method was used to estimate the mean value and standard deviations.

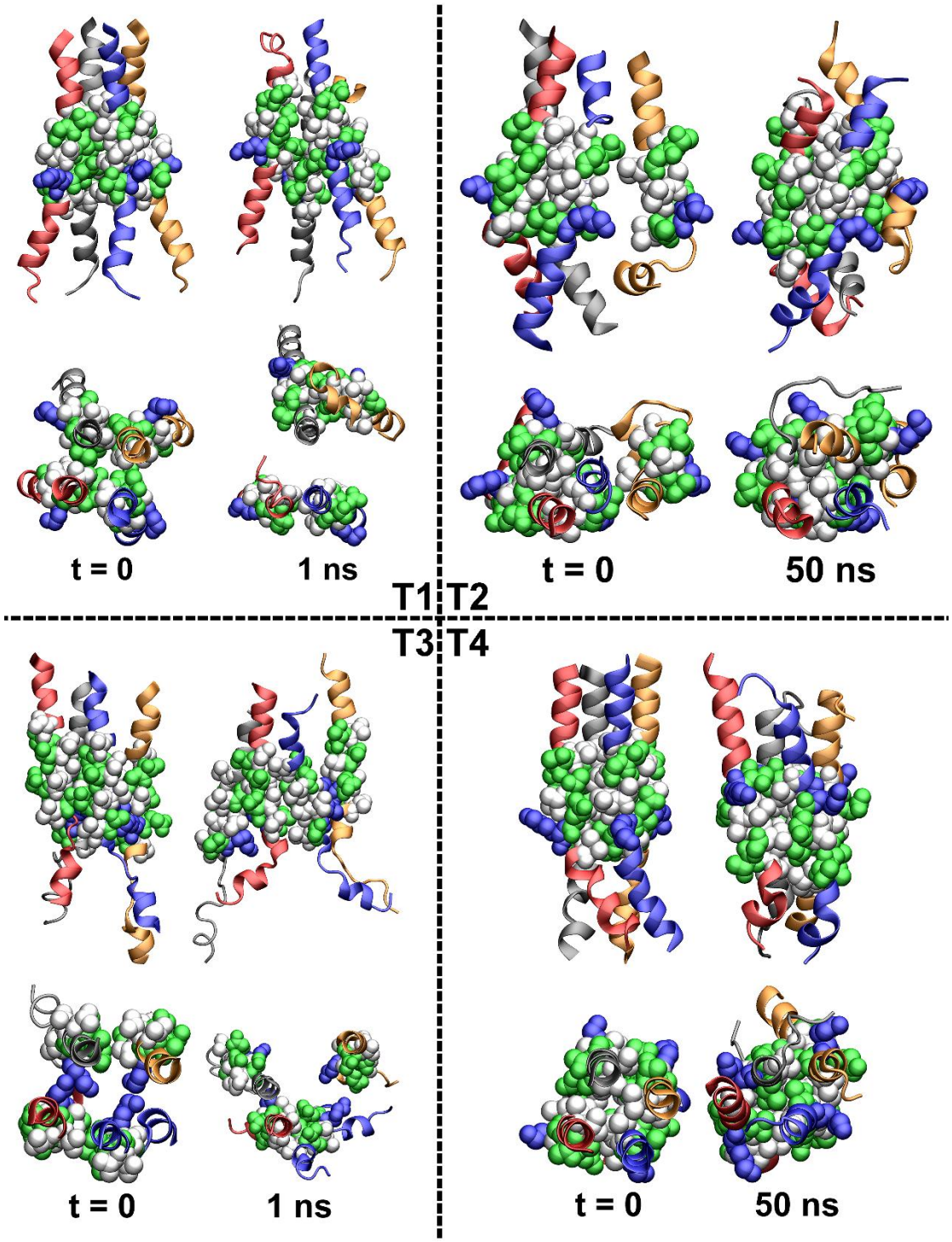

Fig. S1. MD simulations of different helical NAC tetramers T1–T4 in side and top views. The heavy atoms of residues 71–82 are represented as van der Waals spheres with hydrophobic, acidic, basic, and polar residues colored white, red, blue, and green, respectively.

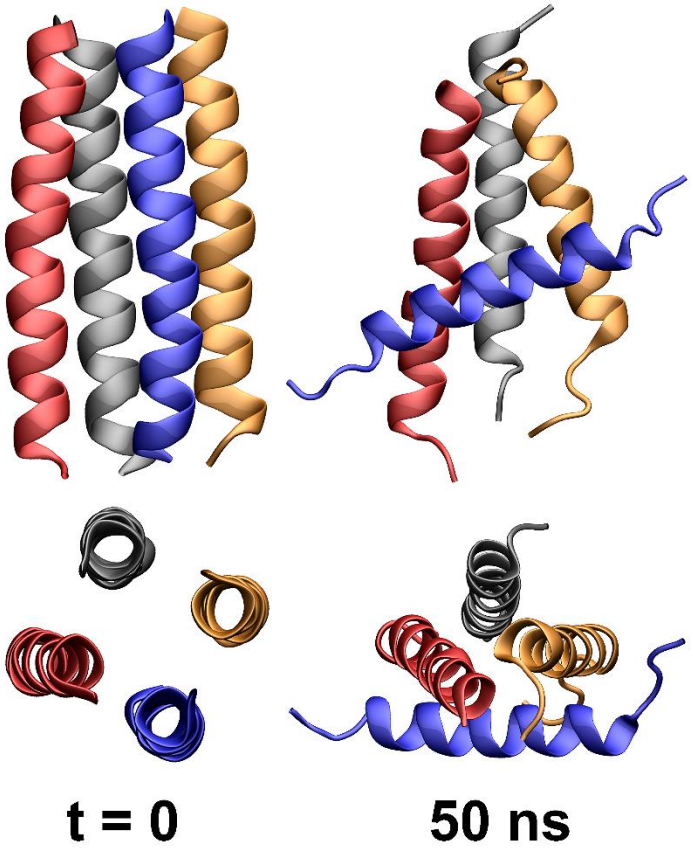

Fig. S2. MD simulations of βS NAC tetramer, approximately corresponding to the **T4** helical αS NAC tetramer with 12 residues deleted (see text). The sequence comparison between αS and βS is shown below.

N-

^{1}MDVFMKGLSKA KEGVV AAAEKTKQGVAEAAGKTKEGVLYVGSKTKEGVVHGVATVAEKTK^{60} **αS**

^{1}MDVFMKGLSMAKEGVVAAAEKTKQGVTEAAEKTKEGVLYVGSKTREGVVQGVASVAEKTK^{60} **βS**

NAC

^{61}EQVTNVGGAV**VTGVTAVAQKTV**EGAGSIAAATGFV^{95} **αS**

^{61}EQASHLGGAVFSG----------AGNIAAATGLVKR^{86} **βS**

C-

^{96}KKDQLGKNEEGAPQEGILEDMPVDPDNEAYEMPSEEGYQDYEPEA^{140} **αS**

^{87}EEFPTDLKPEEVAQEAAEEPLIEPLMEPEGESYEDPPQEEYQEYEPEA^{134} **βS**

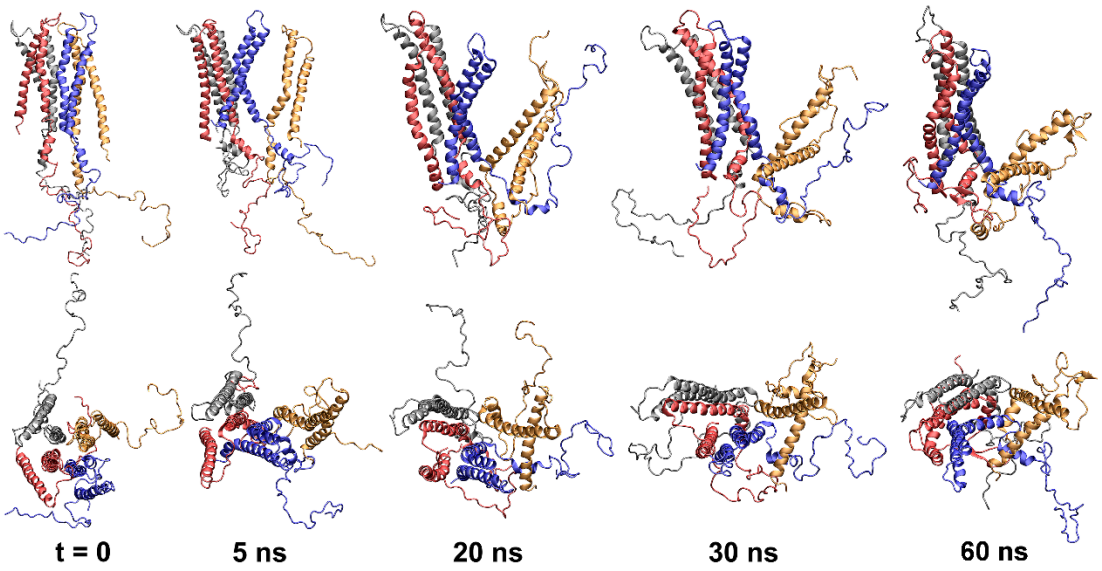

Fig. S3. MD simulations of the tetramer **T3** (the initial structure was provided by Dr. Thomas Pochapsky, based on characterization reported in *Proc. Natl. Acad. Sci. U. S. A.*, 2011, 108, 17797).

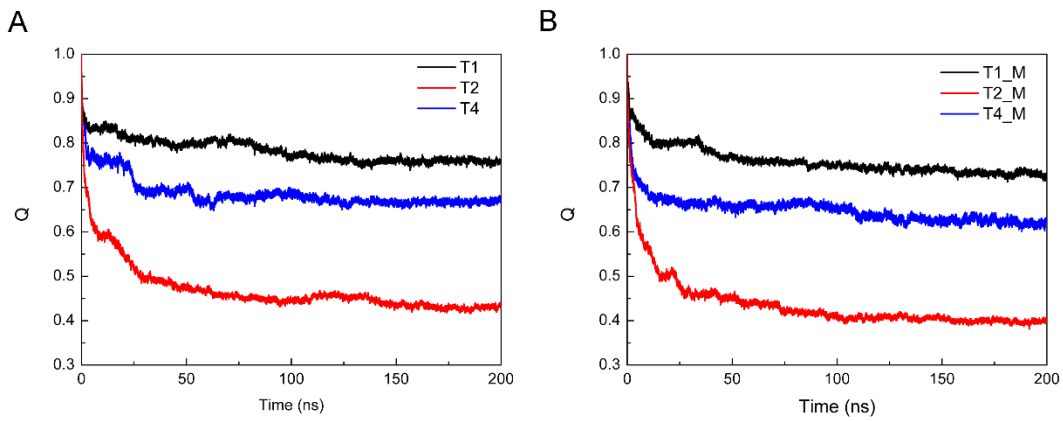

Fig. S4. The fraction of native contacts Q for both wild type (A) and mutated (B) helical αS tetramers. The fraction of native contacts was calculated according to the following formula:

$$\mathrm{Q(X)} = \frac{1}{N}\sum_{(i,j)} \frac{1}{1+\exp[\beta(r_{ij}(X) - \lambda r_{ij}^{0})]}$$

Heavy atoms i and j in residues θ_i and θ_j are in contact if the distance between them is less than 5.0 Å. r_{ij} (X) is the distance between i and j in conformation X; r^0_{ij} (X) is the distance in the native state (starting conformation). β is a smoothing parameter taken to be 5 $Å^{-1}$ and the factor λ accounts for fluctuations when the contact is formed, taken to be 1.8 for the all-atom model. For more details, see *Proc. Natl. Acad. Sci. U. S. A.*, 2013, 110, 17874.

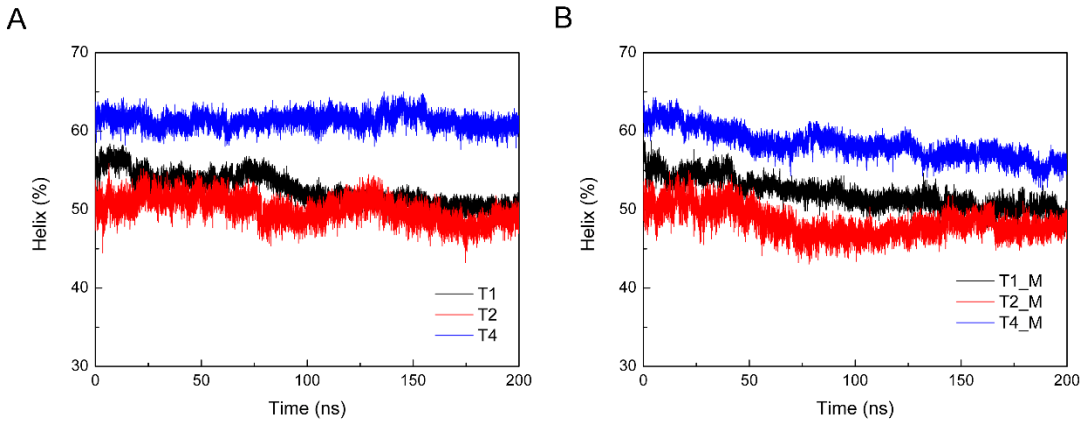

Fig. S5. The time change of helix structures over 200-ns simulations of different wild type (A) and mutated (B) αS tetramers. The percentage of helix is the sum of α-helix, 3_{10}-helix and π-helix as specified in the Define Secondary Structure of Proteins (DSSP) algorithm.

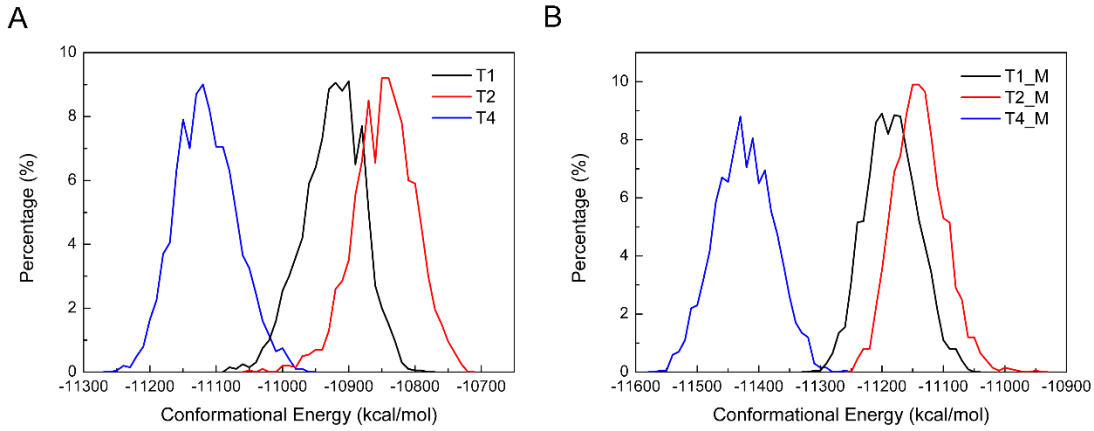

Fig. S6. Distribution of conformational energy (see **Table S1**) calculated for different wild type (A) and mutated (B) αS tetramers.

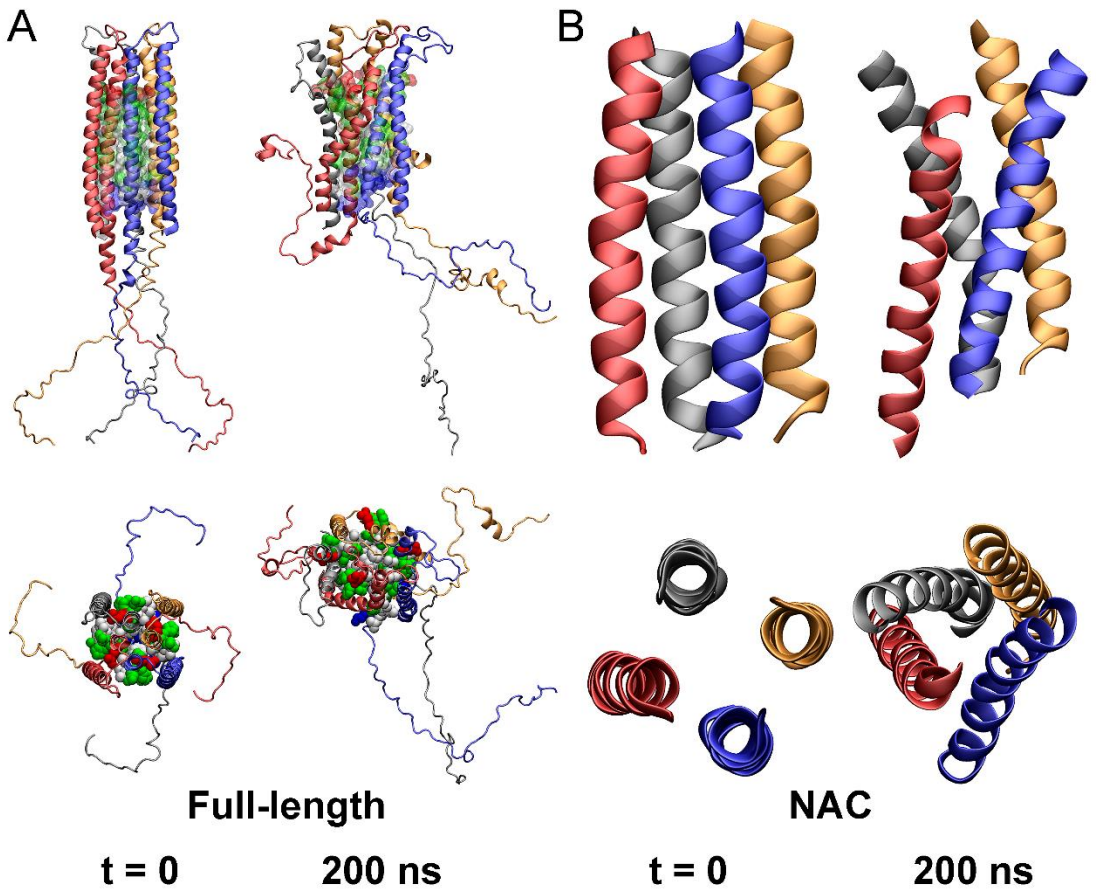

Fig. S7. MD simulations of a βS tetramer. This βS tetramer shares the same α1 and α2 segments as αS tetramer **T4**. (A) Initial and final conformations of the full-length βS tetramer in both side and top views. (B) Initial and final conformations of the NAC region of the βS tetramer in both side and top views.

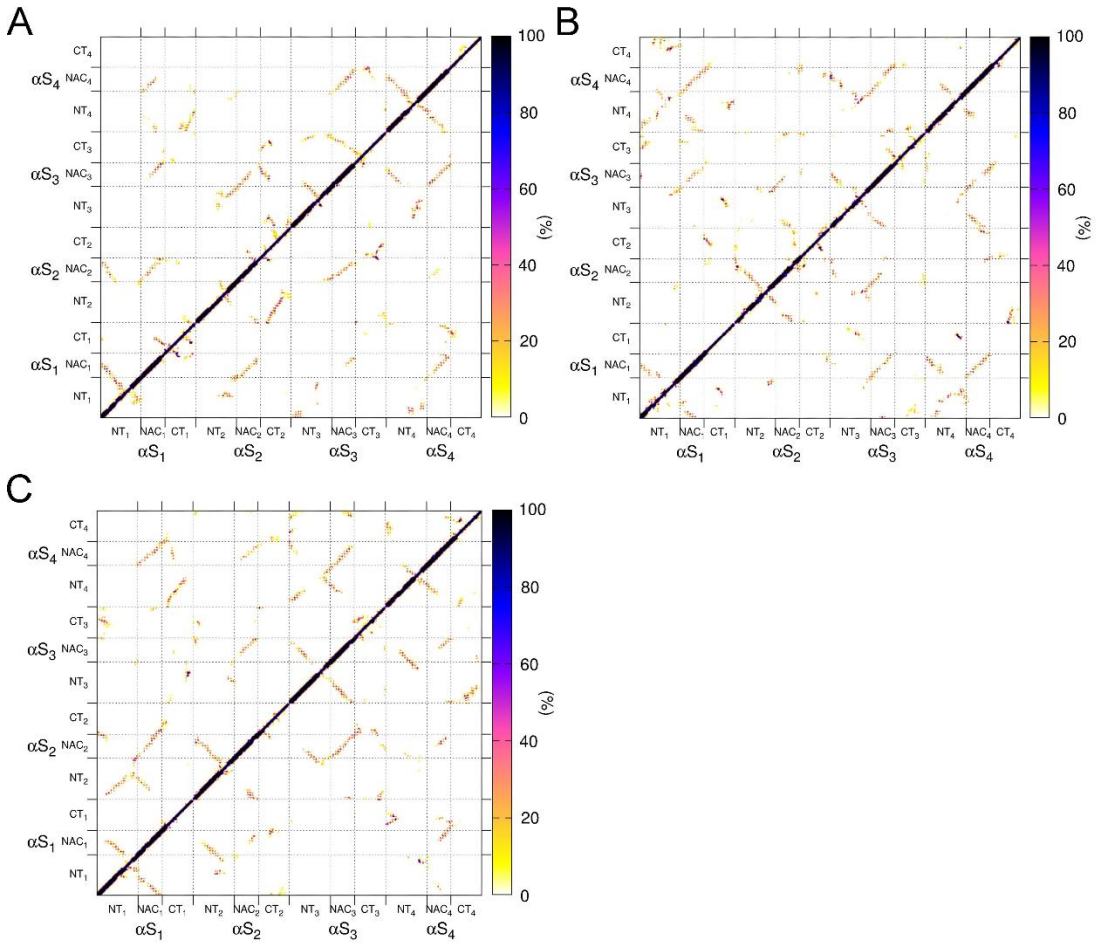

Fig. S8. Contact maps for **T1** (A), **T2** (B), and **T4** (C) tetramers. The contact maps of wild type and mutant are shown in the bottom right and top left half of each figure. Molecular interaction maps were generated by contact analysis. using the CONAN tool.[11] A contact occurs if the distance between any two heavy atoms is within 5 Å.

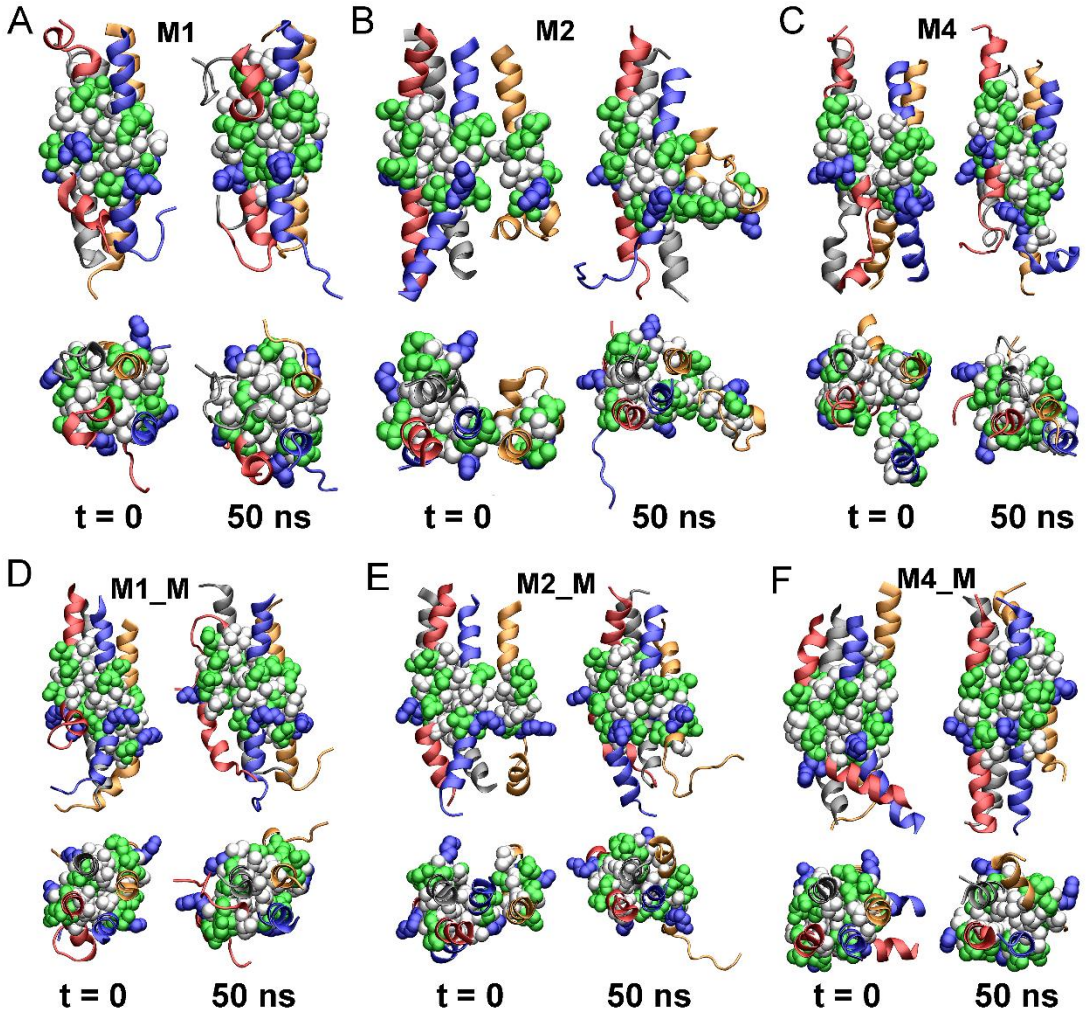

Fig. S9. MD simulations of different helical NAC tetramers with the initial conformations generated from 200-ns simulations of the corresponding full-length αS tetramers. The heavy atoms of residues 71–82 are represented as van der Waals spheres with hydrophobic, acidic, basic, and polar residues colored white, red, blue, and green, respectively.

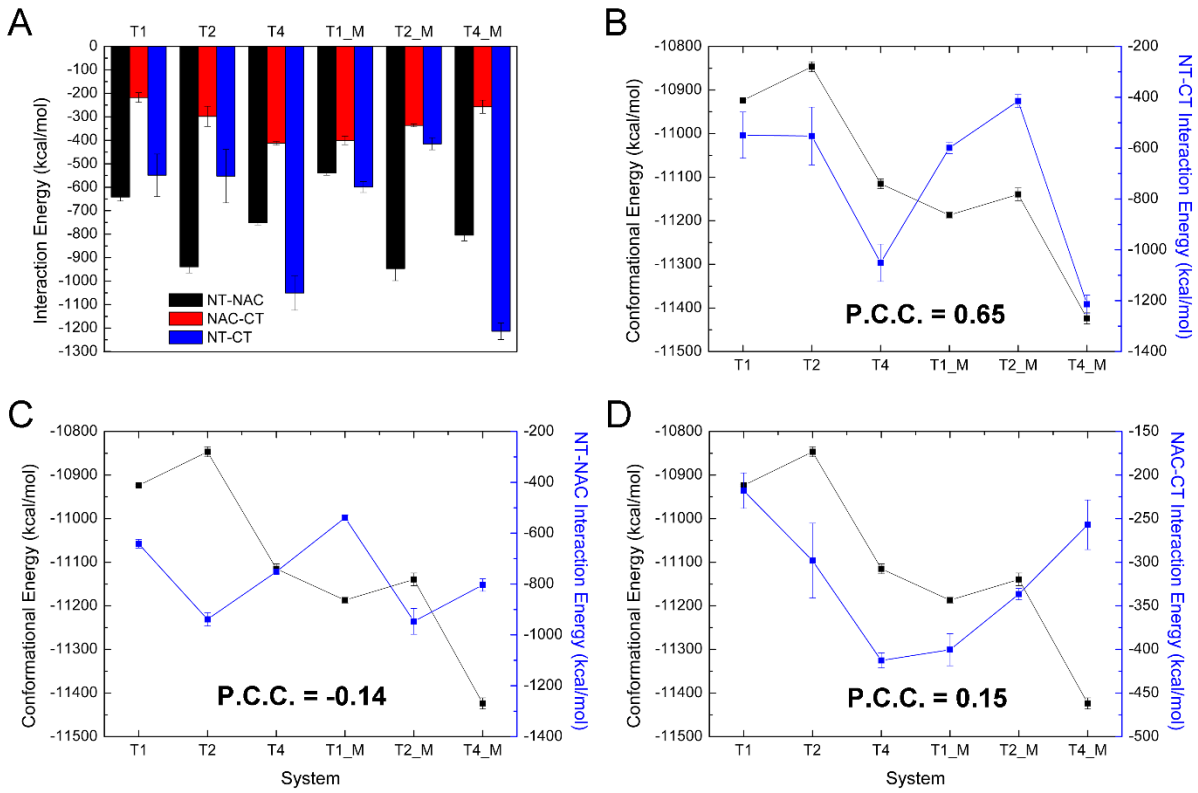

Fig. S10. Interaction energy and Pearson Correlation Coefficient (P.C.C.) between conformational energy and NT-CT, NT-NAC, and NAC-CT interaction energy for different αS tetramers.

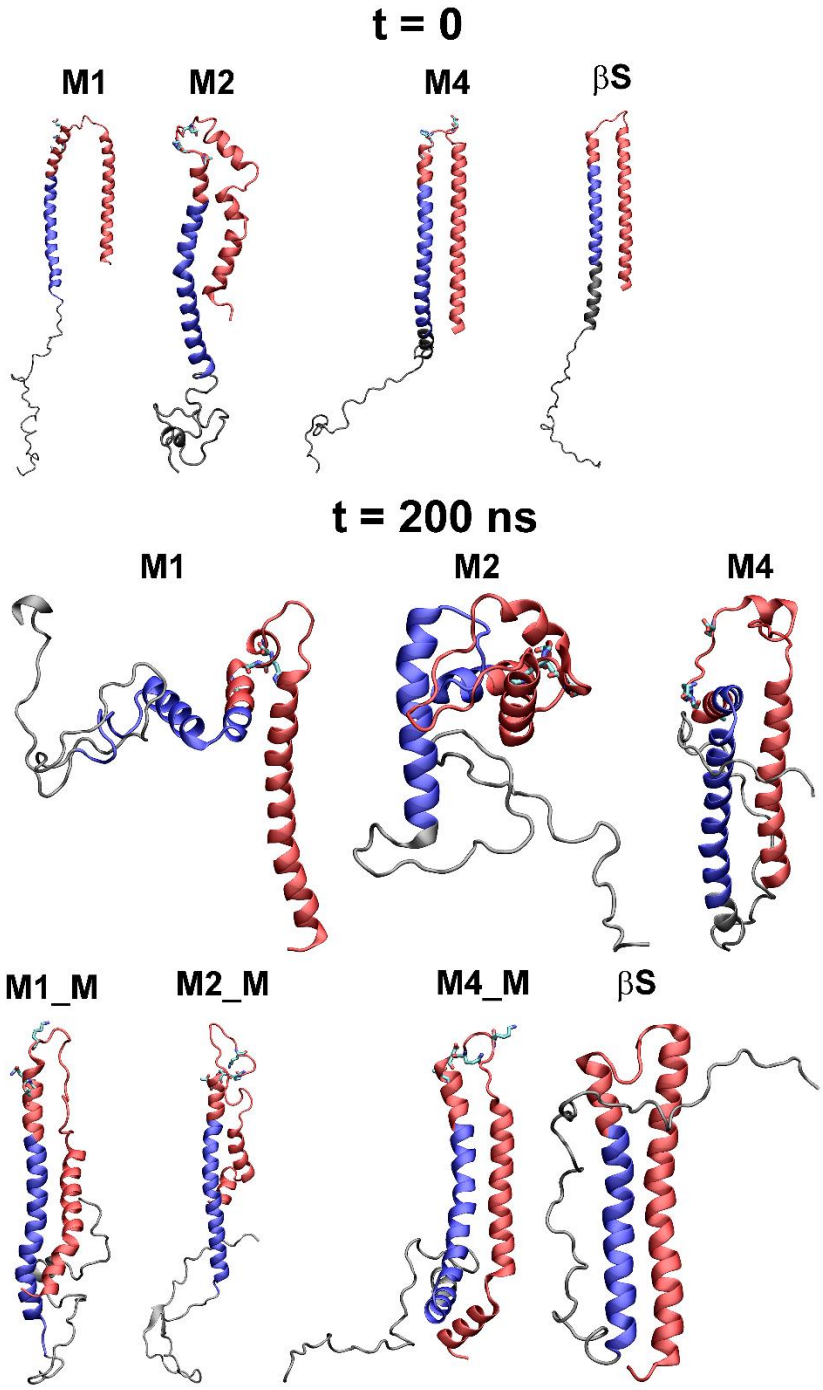

Fig. S11. MD simulations of helical α and β monomers. **M1**, **M2** and **M4** have the same initial conformations as **M1_M**, **M2_M** and **M4_M**, respectively. The N-terminal, NAC region, and C-terminal are colored red, blue and grey, respectively.

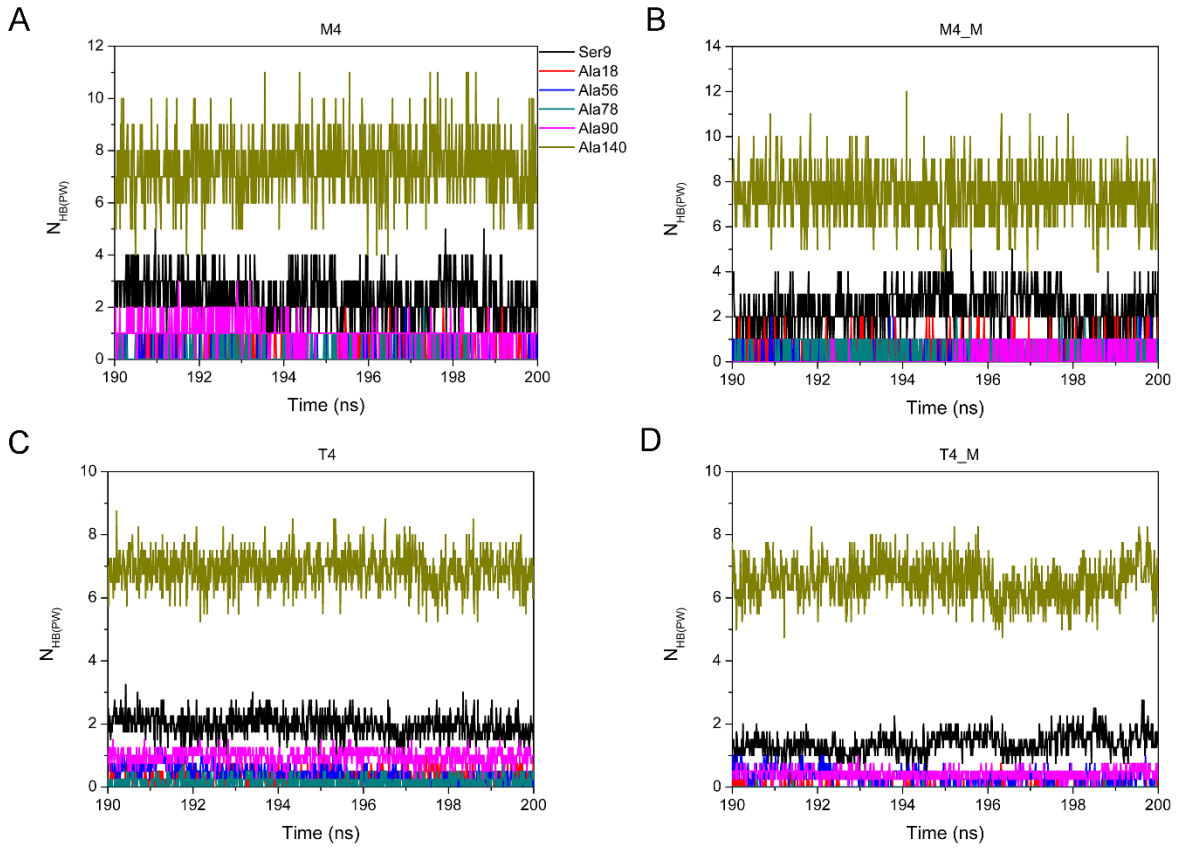

Fig. S12. Number of protein-water hydrogen bonds for residues of interest. These residues were chosen in order to compare their hydration properties with random coil αS monomers reported recently (Biohys. J., 2018, 114, 2540). The number of protein-water hydrogen bonds counts water molecules within 3.5 Å of a specific residue and is averaged over the four monomers.

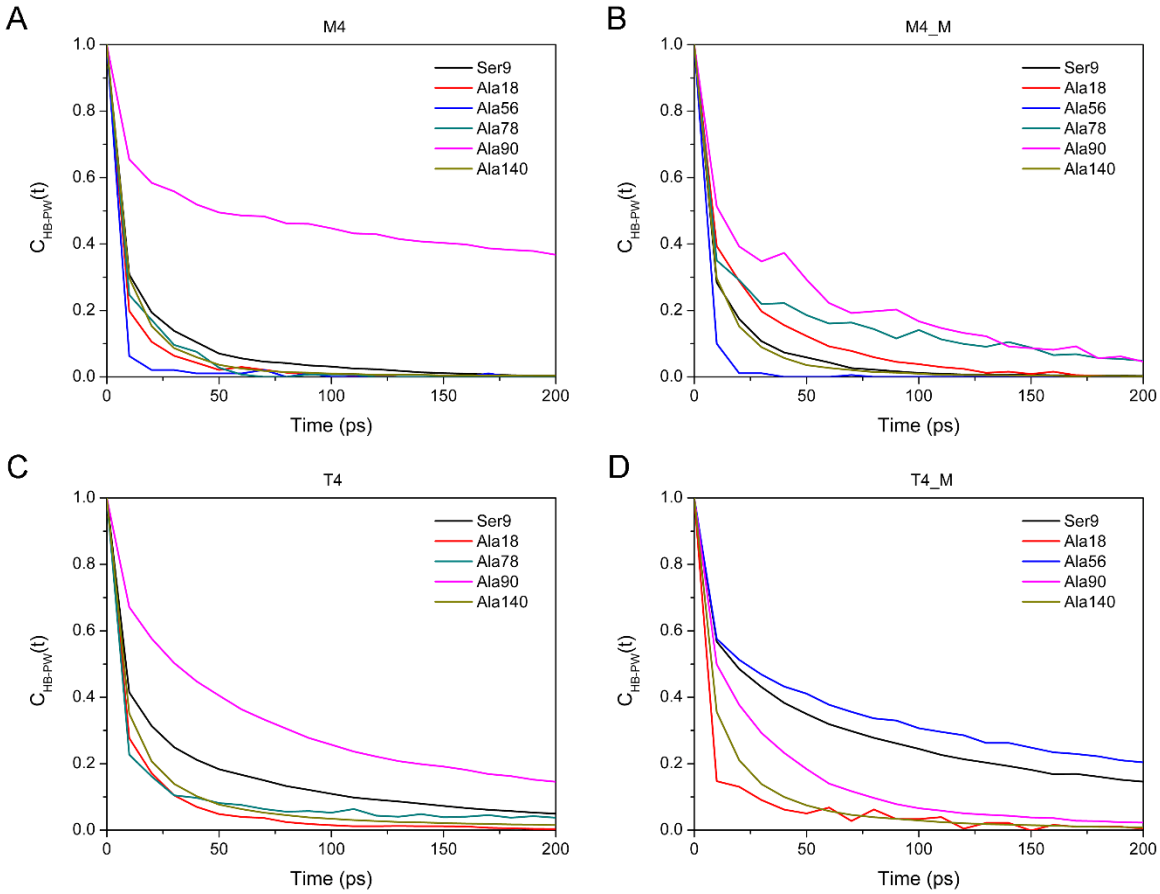

Fig. S13. Correlation functions for protein-water hydrogen bonds.

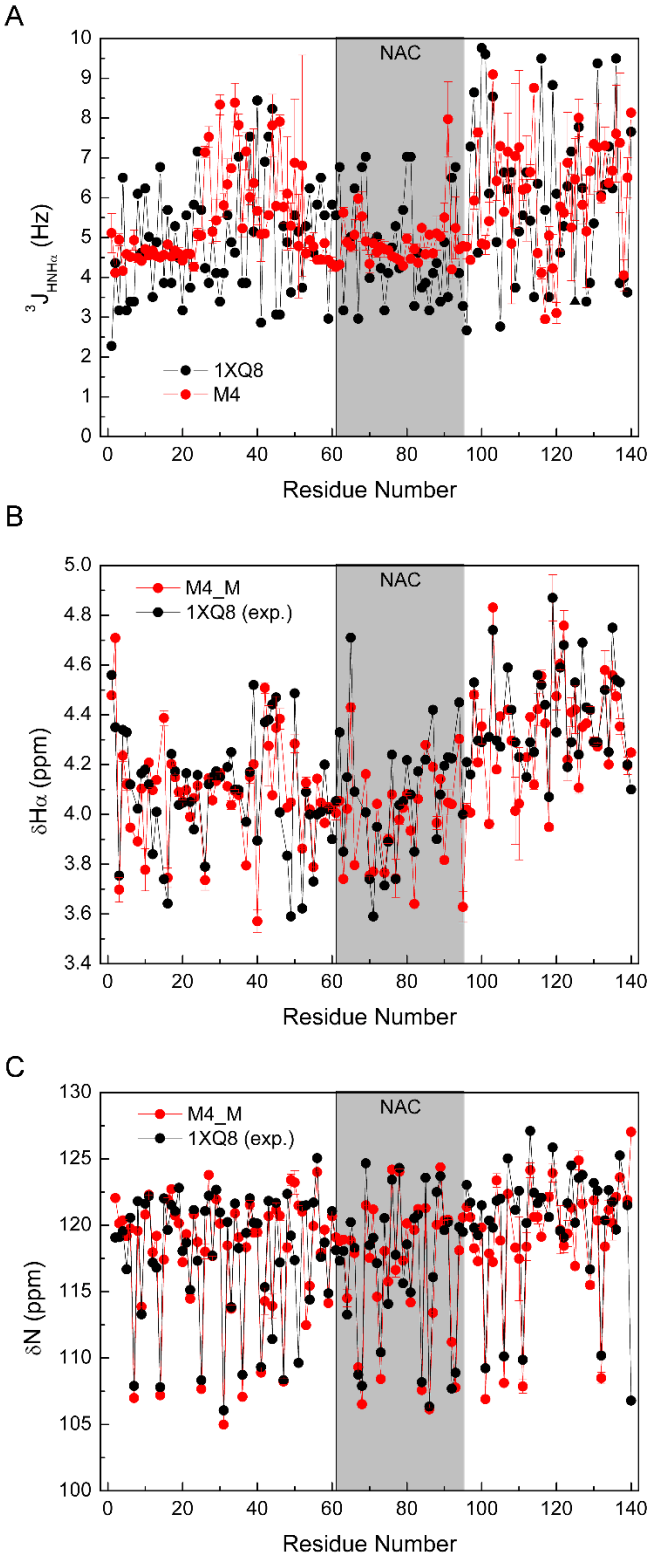

Fig. S14. Comparison of $^3J_{HNH\alpha}$ coupling constants, and Hα and N chemical shifts between the simulation-optimized helical αS structures (M4 and M4_M) and micelle-bound structure (PDB ID: 1XQ8). For details, see Tables S2-S5.

Table S1. Conformational energy (in kcal/mol) calculated using the GBMV implicit solvent model.

System	Total	vdW	Electrostatic	Solvation	Bonded
T1	-10923.7 (1.3)	-1881.7 (15.3)	2028.2 (312.0)	-17102.6 (329.6)	6032.4 (3.6)
T2	-10846.7 (11.4)	-1859.6 (2.6)	1911.0 (313.8)	-16919.5 (298.5)	6021.4 (6.5)
T4	-11115.1 (11.4)	-2014.3 (10.9)	93.3 (157.2)	-15249.1 (175.3)	6054.9 (4.2)
<M1>^{T1}	-2586.0 (23.5)	-338.8 (59.5)	164.4 (344.5)	-3916.2 (366.1)	1504.7 (14.5)
<M2>^{T2}	-2560.6 (11.8)	-319.5 (18.0)	347.6 (110.5)	-4090.0 (65.6)	1501.4 (15.2)
<M4>^{T4}	-2623.1 (2.1)	-358.0 (2.9)	-70.9 (242.8)	-3703.6 (246.4)	1509.4 (12.8)
M1	-2606.8 (6.8)	-374.7 (8.8)	97.8 (246.7)	-3843.5 (245.2)	1513.5 (3.5)
M2	-2617.6 (8.2)	-454.3 (11.9)	-359.9 (15.7)	-3336.6 (20.9)	1533.2 (8.8)
M4	-2647.9 (15.8)	-408.5 (2.1)	-436.3 (23.4)	-3315.6 (43.6)	1512.6 (2.3)
M1^{first}	-2563.2 (26.7)	-280.8 (5.4)	602.3 (168.8)	-4384.9 (142.9)	1500.2 (4.7)
M2^{first}	-2540.5 (3.0)	-332.8 (22.6)	318.4 (244.5)	-4073.2 (240.4)	1547.2 (15.5)
M4^{first}	-2636.9 (0.1)	-334.6 (5.9)	280.8 (31.7)	-4073.5 (37.2)	1490.5 (11.5)
T1_M	-11187.0 (6.6)	-1770.1 (24.3)	1430.9 (296.9)	-16965.6 (290.8)	6116.7 (11.6)
T2_M	-11139.3 (14.7)	-1875.1 (15.9)	3126.1 (68.1)	-18534.0 (86.6)	6143.8 (17.2)
T4_M	-11423.9 (12.8)	-1982.6 (10.1)	-1261.1 (68.9)	-14339.3 (94.3)	6159.1 (2.5)
<M1_M>^{T1_M}	-2682.1 (55.0)	-332.3 (16.6)	123.1 (192.4)	-3998.3 (171.8)	1525.4 (17.8)
<M2_M>^{T2_M}	-2649.4 (0.6)	-323.1 (19.2)	444.6 (38.4)	-4302.7 (59.5)	1531.8 (6.5)
<M4_M>^{T4_M}	-2696.7 (10.8)	-327.9 (3.6)	14.6 (201.8)	-3917.0 (197.5)	1533.4 (7.8)
M1_M	-2740.3 (0.6)	-409.0 (10.9)	-406.7 (88.3)	-3460.6 (86.8)	1536.1 (11.7)
M2_M	-2707.1 (8.2)	-388.2 (9.1)	-101.0 (39.3)	-3742.1 (37.1)	1524.2 (15.1)
M4_M	-2751.2 (3.0)	-400.0 (6.2)	-329.2 (128.7)	-3555.3 (117.5)	1533.3 (14.3)
M1_M^{first}	-2680.5 (9.1)	-283.4 (12.8)	527.5 (8.8)	-4446.1 (13.7)	1521.4 (1.1)
M2_M^{first}	-2676.1 (14.6)	-357.3 (18.6)	277.0 (92.0)	-4144.0 (72.9)	1548.3 (14.1)
M4_M^{first}	-2754.5 (3.6)	-342.5 (7.2)	69.1 (89.2)	-4008.4 (82.3)	1527.3 (3.9)
$\beta S^{tetramer}$	-12777.4 (19.5)	-1736.9 (0.9)	7470.7 (429.3)	-24600.7 (422.6)	6089.6 (25.3)
<$\beta S^{monomer}$>	-2931.9 (22.5)	-316.7 (34.5)	627.4 (267.7)	-4761.8 (248.2)	1519.2 (22.3)
$\beta S^{monomer}$	-2980.8 (0.8)	-395.7 (6.7)	297.5 (35.8)	-4406.3 (32.6)	1523.7 (9.0)

Notes: (1) The net charge decreases by -1e and -4e for mutated monomer and tetramer, respectively.

(2) The conformational energy refers to the total energy shown in the table.

(3) <. > indicates energy averaged over the four monomers within a tetramer.

(4) ^{first} indicates energy calculated based on the first 10 ns trajectory due to fast conformational change in M1 and M2, otherwise, last 20 ns.

Table S2. Pearson Correlation Coefficient (P.C.C.) of J-coupling constants between different systems.

$^3J_{HNH\alpha}$	1XQ8 (sim.)	M4	M4_M	<M4>^{T4}	<M4_M>^{T4}
1XQ8 (sim.)	1.00	**0.05**	0.22	0.10	0.21
M4	**0.05**	1.00	0.35	0.55	0.55
M4_M	0.22	0.35	1.00	0.65	0.60
<M4>^{T4}	0.10	0.55	0.65	1.00	0.68
<M4_M>^{T4_M}	0.21	0.55	0.60	0.68	1.00

Table S3. Pearson Correlation Coefficient (P.C.C.) of Cα chemical shifts between different systems.

δCα	1XQ8 (exp.)	M4	M4_M	<M4>^{T4}	<M4_M>^{T4}
1XQ8 (exp.)	1.00	0.99	0.97	0.98	0.97
M4	0.99	1.00	0.98	0.99	0.97
M4_M	0.97	0.98	1.00	0.97	0.99
<M4>^{T4}	0.98	0.99	0.97	1.00	0.97
<M4_M>^{T4_M}	0.97	0.97	0.99	0.97	1.00

Table S4. Pearson Correlation Coefficient (P.C.C.) of Hα chemical shifts between different systems.

δHα	1XQ8 (exp.)	M4	M4_M	<M4>^{T4}	<M4_M>^{T4}
1XQ8 (exp.)	1.00	0.98	**0.79**	0.82	0.84
M4	0.98	1.00	0.81	0.84	0.87
M4_M	**0.79**	0.81	1.00	0.86	0.84
<M4>^{T4}	0.82	0.84	0.86	1.00	0.89
<M4_M>^{T4_M}	0.84	0.87	0.84	0.89	1.00

Table S5. Pearson Correlation Coefficient (P.C.C.) of N chemical shifts between different systems.

δN	1XQ8 (exp.)	M4	M4_M	<M4>^{T4}	<M4_M>^{T4}
1XQ8 (exp.)	1.00	0.90	**0.83**	0.89	0.85
M4	0.90	1.00	0.91	0.95	0.91
M4_M	**0.83**	0.91	1.00	0.90	0.95
<M4>^{T4}	0.89	0.95	0.90	1.00	0.92
<M4_M>^{T4_M}	0.85	0.91	0.95	0.92	1.00

Notes: (1) The chemical shits were calculated using SHIFTX2 program[12] for conformations from the last 20-ns MD trajectories. The NMR J-coupling constants were calculated using the Karplus equation (g_chi tool in Gromacs software).

(2) 1XQ8 (sim.) refers to the calculated J-coupling constant for micelle-bound αS (PDB ID: 1XQ8); and 1XQ8 (exp.) refers to the experimental chemical shift for the same micelle-bound αS (PDB ID: 1XQ8).

(3) M4, M4_M, <M4>^{T4}, and <M4_M>^{T4_M} refer to the systems shown in **Table S1**.

(4) Compared to experimental structure 1XQ8, the designed helical αS (M4) has the biggest difference in ^{3}J-coupling constant; and the mutant (M4_M) has the biggest difference in Hα and N chemical shifts (shown in **Fig. S14**).

Supplementary References

1. T. S. Ulmer, A. Bax, N. B. Cole and R. L. Nussbaum, *J. Biol. Chem.*, 2004, **280**, 9595-9603.
2. T. Gurry, O. Ullman, C. K. Fisher, I. Perovic, T. Pochapsky and C. M. Stultz, *J. Am. Chem. Soc.*, 2013, **135**, 3865-3872.
3. W. Wang, I. Perovic, J. Chittuluru, A. Kaganovich, L. T. T. Nguyen, J. Liao, J. R. Auclair, D. Johnson, A. Landeru, A. K. Simorellis, S. Ju, M. R. Cookson, F. J. Asturias, J. N. Agar, B. N. Webb, C. Kang, D. Ringe, G. A. Petsko, T. C. Pochapsky and Q. Q. Hoang, *Proc. Natl. Acad. Sci. U. S. A.*, 2011, **108**, 17797-17802.
4. E. Kara, P. A. Lewis, H. Ling, C. Proukakis, H. Houlden and J. Hardy, *Neurosci. Lett.*, 2013, **546**, 67-70.
5. J. Huang, S. Rauscher, G. Nawrocki, T. Ran, M. Feig, B. L. de Groot, H. Grubmüller and A. D. MacKerell, *Nat. Methods*, 2016, **14**, 71-73.
6. M. J. Abraham, T. Murtola, R. Schulz, S. Páll, J. C. Smith, B. Hess and E. Lindahl, *SoftwareX*, 2015, **1-2**, 19-25.
7. G. Bussi, D. Donadio and M. Parrinello, *J. Chem. Phys.*, 2007, **126**, 014101.
8. M. Parrinello and A. Rahman, *J. App. Phys.*, 1981, **52**, 7182-7190.
9. B. R. Brooks, R. E. Bruccoleri, B. D. Olafson, D. J. States, S. Swaminathan and M. Karplus, *J. Comput. Chem.*, 1983, **4**, 187-217.
10. (*a*) M. S. Lee, F. R. Salsbury and C. L. Brooks, *J. Chem. Phys.*, 2002, **116**, 10606-10614; (*b*) M. S. Lee, M. Feig, F. R. Salsbury and C. L. Brooks, *J. Comput. Chem.*, 2003, **24**, 1348-1356; (*c*) M. Feig, A. Onufriev, M. S. Lee, W. Im, D. A. Case and C. L. Brooks, *J. Comput. Chem.*, 2004, **25**, 265-284.
11. D. Mercadante, F. Gräter and C. Daday, *Biophys. J.*, 2018, **114**, 1267-1273.
12. B. Han, Y. Liu, S. W. Ginzinger and D. S. Wishart, *J. Biomol. NMR*, 2011, **50**, 43-57.